Geochemical Perspectives Letters

Dominance of benthic flux of REEs on continental shelves: implications for oceanic budgets

K. Deng[1,2*], S. Yang[2], J. Du[1], E. Lian[2], D. Vance[1]

OPEN ACCESS

https://doi.org/10.7185/geochemlet.2223

Abstract

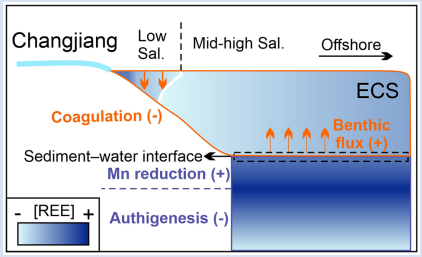

Rare earth elements (REEs) are powerful tools to track oceanic biogeochemical processes. However, our understanding of REE sources is incomplete, leading to controversial interpretations regarding their oceanic cycling. Continental margin sediments are often assumed to be a major source, but the sediment pore water data required to understand the processes controlling that potential source are scarce. Here, we measure and compile pore water and estuarine REE data from the Changjiang (Yangtze) estuary–East China Sea shelf. We show that release of REEs, from shallow pore water to overlying seawater, is coupled to Mn reduction. In contrast, REEs are removed in deep pore water, perhaps via formation of an authigenic REE-bearing phase. This sedimentary source can potentially explain REE addition in the estuary at mid-high salinity. Our calculations suggest that the benthic flux is the largest Nd source (~40 %) on the East China Sea shelf. Globally, however, despite a higher benthic Nd flux on the advection-dominated shelf, the much more extensive deep ocean still dominates the total area-integrated benthic flux. Our results call for a more extensive investigation of the magnitude of the benthic flux of REEs to the oceans.

Received 8 March 2022 | Accepted 8 June 2022 | Published 30 June 2022

Introduction

The rare earth elements (REEs), as a series of particle-reactive elements, show non-conservative behaviour during transport from continental source to oceanic sink (Elderfield and Greaves, 1982; Rousseau *et al.*, 2015). As such, REE patterns are widely used in oceanographic studies, to track boundary exchange and internal cycling (Elderfield and Greaves, 1982; Jeandel and Oelkers, 2015). Nevertheless, source-to-sink processes for oceanic REEs remain poorly understood. Two hypotheses have been proposed to explain oceanic REE distributions: the top-down (Siddall *et al.*, 2008) *versus* the bottom-up control (Abbott *et al.*, 2015; Du *et al.*, 2020). The former emphasises reversible scavenging, while the latter focuses on the dominance of benthic processes. The resolution of this debate would provide valuable insights on the long-standing "Nd (Neodymium) paradox": while Nd isotopes appear to behave conservatively during water mass mixing, dissolved Nd concentrations ($[Nd]_{diss}$) reflect the behaviour of a reactive element (Arsouze *et al.*, 2009; Haley *et al.*, 2017). Such inconsistency impedes the application of Nd isotopes as a tracer for paleo-circulation (Du *et al.*, 2020; Patton *et al.*, 2021).

The ambiguities in the oceanic REE cycling and budget are partially caused by incomplete understanding of REE sources. The mass balance of oceanic REEs requires sources other than riverine input and atmospheric deposition (Elderfield and Greaves, 1982), such as a benthic dissolved flux across the sediment–water interface via porewater (Abbott *et al.*, 2015; Du *et al.*, 2016) and/or submarine groundwater discharge (Johannesson *et al.*, 2011). In particular, recent modelling efforts suggest that continental margin sediments can be a major source of oceanic REEs (Arsouze *et al.*, 2009; Rempfer *et al.*, 2011). On continental margins, isolating the contribution of a sedimentary REE flux to seawater is particularly difficult because of the complex interaction between riverine input, oceanic currents, and benthic processes. Dissolved REEs have been measured in many estuarine transects and an additional sedimentary source is often proposed to explain their spatial distribution (Wang and Liu, 2008; Rousseau *et al.*, 2015). However, the corresponding sediment porewater REE data, which provide the direct evidence for a benthic flux, are still scarce.

Here, we focus on one of the largest land–ocean interfaces in Asia, the Changjiang (Yangtze) River–East China Sea system. The Changjiang River delivers a huge amount of fresh water (~890 km^3/yr) and sediment (~450 Mt/yr) to the continental margin (Chen *et al.*, 2001), accounting for 2–3 % of global discharge. The East China Sea is characterised by one of the widest continental shelves (shelf area: ~5×10^5 km^2) and highest sedimentation rate (inner shelf: ~1–6 cm/yr) worldwide (Liu *et al.*, 2006). The high dissolved–particulate riverine fluxes make this region ideal for studying the effect of boundary exchange on REE cycling. This paper presents REE data for shelf sediment porewater profiles, as well as for estuarine water from this study and the literature. The main aim is to investigate REE cycling on the East China Sea shelf, with an emphasis on benthic processes,

1. Institute of Geochemistry and Petrology, Department of Earth Sciences, ETH Zürich, Clausiusstrasse 25, 8092 Zürich, Switzerland
2. State Key Laboratory of Marine Geology, Tongji University, 200092 Shanghai, China
* Corresponding author (email: kai.deng@erdw.ethz.ch; 103459@tongji.edu.cn)

and to provide new insights on the role of the continental shelf in the global benthic REE flux.

REE Cycling on the Shelf

Along the salinity transect in the Changjiang estuary, estuarine $[REE]_{diss}$ decreases dramatically at salinity <1–2 psu, driven by scavenging, and gradually increases at mid-high salinity (Fig. S-3), hinting at a potential marine sedimentary source (Wang and Liu, 2008). We measured porewater $[REE]_{diss}$ for four multi-core stations at water depths of 6–46 m (Figs. 1, 2; locations in Fig. S-1). $[REE]_{diss}$ of shallow porewater is generally higher than that for bottom water, consistent with observations from other continental margins and with release of porewater REEs to the overlying seawater (Haley *et al.*, 2004; Abbott *et al.*, 2015).

At the shallowest site, C6-1 at 6 m, the REE patterns are relatively invariant (Fig. 1). However, porewater $[REE]_{diss}$ increases with core depth, implying a diagenetic source below the studied depth range and upward diffusion. The similarity between the porewater $[Mn]_{diss}$ and $[REE]_{diss}$ profiles (Fig. 2) at C6-1 suggests a source of both at depths at, or beneath, ~20 cm, most likely the reductive dissolution of Mn oxides. Porewaters at C10 (depth: 12 m) are characterised by a maximum in $[REE]_{diss}$ at shallow core depth (<7 cm), coincident with a maximum in $[Mn]_{diss}$ (Fig. 2). These observations are again consistent with a source of REE linked to Mn reduction. Indeed, REEs are commonly enriched in Mn oxides and they can be released together in a reductive environment (Blaser *et al.*, 2016). The change in porewater REE patterns also supports the control of Mn reduction. The correlation ($R^2 = 0.58$; <7 cm at C10; Fig. S-4) between porewater $[Mn]_{diss}$ and Ce anomaly (Ce/Ce^*) values (Eq. S-1) is consistent with the well-known association of Ce with Mn oxyhydroxide (Schijf *et al.*, 2015). Besides, the Mn-Fe leachate from the Changjiang sediment with low ratios of heavy REEs to light REEs (HREE/LREE, Eq. S-2; <1 when normalised to the post-Archean Australian Shale or PAAS) (Wang and Liu, 2008) would release more dissolved LREEs (relative to bottom water) as observed (Fig. 1). In comparison, $[Fe]_{diss}$ is generally low (mostly <1 μM) throughout core C6-1 and at shallow depth in C10, and the highest $[Fe]_{diss}$ of all cores (at 16 cm of C10) corresponds to the lowest $[Nd]_{diss}$ in this core. Hence, either Fe cycling is not the major controlling factor of REEs in either core, or its effect is obscured by other factors.

At depths exceeding ~7 cm in C10, $[LREE]_{diss}$ decreases dramatically, accompanied by an HREE-enriched pattern (Fig. 1). This evolution with depth hints at the operation of a second early diagenetic process. Here, lower $[REE]_{diss}$ and preferential scavenging of LREEs suggest removal to an authigenic phase. High porewater $[P]_{diss}$ at depth (13–24 μM), in contrast to ~1 μM at <4 cm (Fig. 2), could facilitate the precipitation of minor phosphate (Byrne and Kim, 1993). This is consistent with in-situ formation of authigenic P at great sediment depth in this region (Liu *et al.*, 2020), and with the fact that phosphate precipitation would result in an HREE-enriched pattern in solution (Byrne and Kim, 1993).

More LREEs release at shallow core depth and preferential removal at great core depth can also be observed at greater water depth (33 m at C13 and 46 m at B14) (Fig. 1). Specifically, peaks in $[Mn]_{diss}$ and $[Nd]_{diss}$ are co-located at shallow core depth (≤6 cm; Fig. 2). $[Fe]_{diss}$ also peaks at ≤6 cm and thus its effect on $[Nd]_{diss}$ is difficult to isolate. For both stations, $[Nd]_{diss}$ becomes much lower at great depths (>7 cm) while $[P]_{diss}$ remains high (>10 μM). Note that the clear association of high porewater REE abundance and release of more LREEs (relative to bottom water) with Mn reduction could be obscured sometimes: REE concentrations and patterns reflect the competition between diverse sources and sinks, and the contribution of each component likely varies among basins (Haley *et al.*, 2004; Abbott *et al.*, 2015).

To further illustrate REE cycling through the Changjiang Estuary–East China Sea transect, we present the relationship between Ce/Ce^* and HREE/LREE (Fig. 3). Estuarine scavenging leads to a decrease in Ce/Ce^* and an increase in HREE/LREE

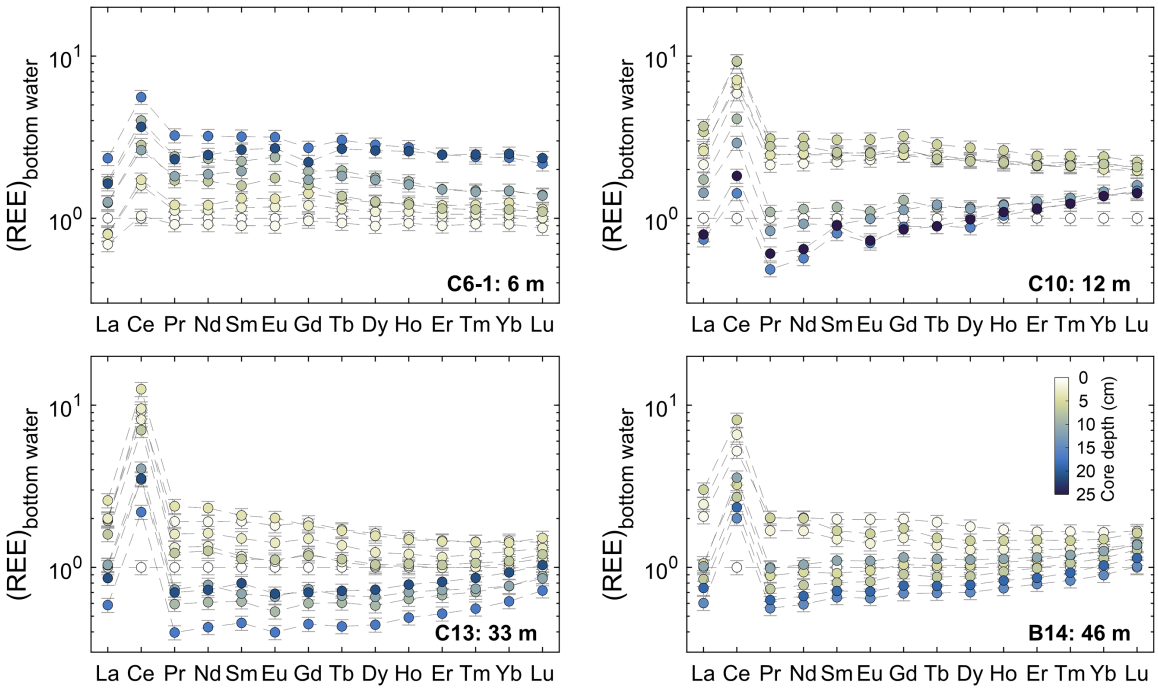

Figure 1 Sediment porewater REE pattern normalised to the bottom seawater (depth of 0 cm) at each station. Analytical uncertainties (see Supplementary Information) are shown here and in later figures.

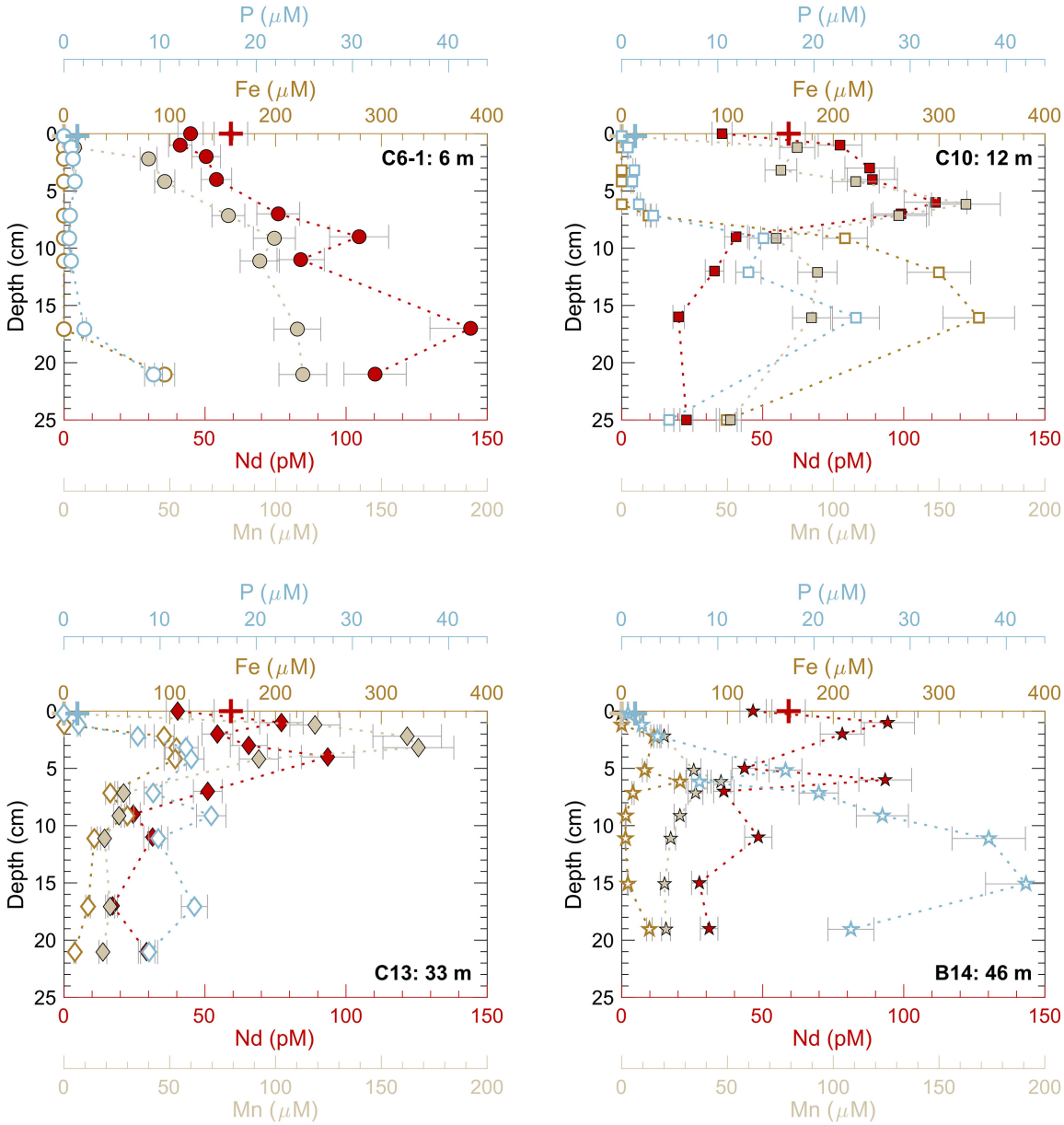

Figure 2 Porewater and bottom seawater (depth of 0 cm) Nd, Mn (filled symbols), Fe and P (open symbols) concentrations. "+" symbols refer to the water sample data at station C1 at 1 m.

(towards seawater end members), while the reductive release of REEs in shallow porewater shows a reverse trend, with lower HREE/LREE and higher Ce/Ce* (towards Mn-Fe leachate). At greater core depth, the REE patterns deviate from those controlled by these two processes and are characterised by a sharp rise in HREE/LREE and only a slight decrease in Ce/Ce*, suggesting the operation of a different process (authigenesis).

Implications for Nd Budget in the Marginal Sea and Global Oceans

Our data are clearly consistent with the interaction between REE scavenging in the estuary and reductive REE release from shallow sediments. We calculate the diffusive Nd flux from sediments based on porewater $[Nd]_{diss}$ gradient (Eq. S-5). The diffusive Nd flux is lowest (0.9 pmol/cm^2/yr) at 6 m and increases to a stable level at 6.0 ± 0.8 pmol/cm^2/yr (12–46 m). Figure 4 compares these diffusive fluxes with compiled literature porewater data. Our dataset falls within the global trend (Du *et al.*, 2018, 2020), which shows higher fluxes in the deeper ocean (R^2 = 0.30). Furthermore, there is no clear control of bottom dissolved oxygen (DO) on diffusive Nd flux (Abbott *et al.*, 2015), with no correlation between the two (Fig. 4; p = 0.26). The spatial trend of diffusive Nd flux is probably affected by multiple depth-related processes. At shallow water depths the exchange between porewater and overlying seawater is fast (Shi *et al.*, 2019; Patton *et al.*, 2021), resulting in a small Nd gradient at sediment–water interface. In comparison, in some deep ocean sediments high reactive authigenic [Nd] might contribute to a high benthic flux (Abbott *et al.*, 2016; Haley *et al.*, 2017).

To estimate the contribution of benthic processes to the Nd budget in the East China Sea shelf, Nd fluxes of all major sources need to be known (Table S-5), including the Changjiang River, atmospheric deposition, the Taiwan Strait Current, the Kuroshio Current intrusion (Liu *et al.*, 2021) and shelf benthic flux. The Changjiang-derived Nd flux (after

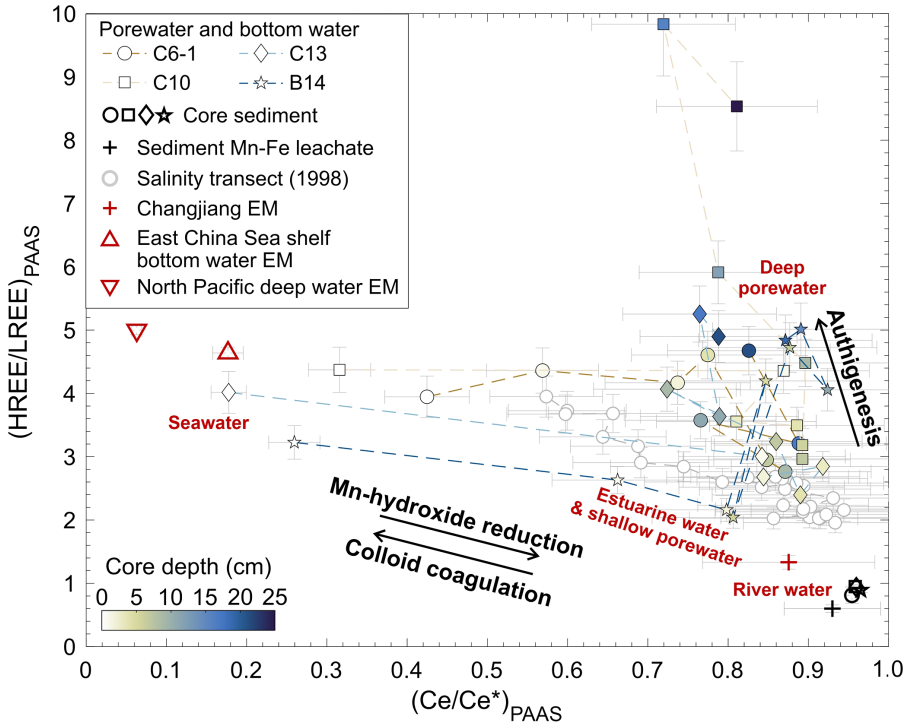

Figure 3 Shelf REE cycling shown by a Ce/Ce*-HREE/LREE plot. REE data for the salinity transect (1998) and Mn-Fe leachate are from Wang and Liu (2008). The data source for water mass end members (EMs) is provided in Figure S-3.

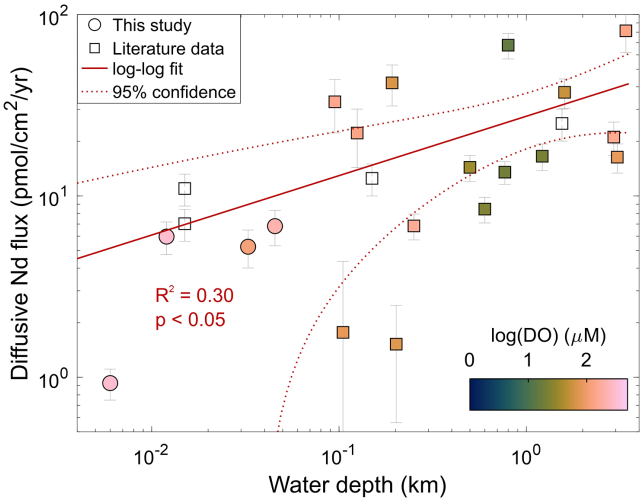

Figure 4 Diffusive sedimentary Nd flux variation with depth. The coloured symbols indicate bottom water DO and open symbols are those with no DO data available. Axes and colour bar are on log scale. Compiled dataset and references are provided in Table S-4.

estuarine scavenging) and the atmospheric input are $2.7 \pm 0.4 \times 10^4$ mol/yr and $1.7 \pm 0.4 \times 10^4$ mol/yr, respectively. In comparison, Nd fluxes from the Taiwan Strait Current and the intrusion of the Kuroshio Current are much higher at $21.6 \pm 3.8 \times 10^4$ mol/yr and $25.2 \pm 4.4 \times 10^4$ mol/yr, respectively (Table S-5). Given the similar porewater REE behaviours (Fig. 1) and small flux variability (Table S-4) at depth of ≥12 m, we use the average diffusion-based flux estimate (6.0 pmol/cm^2/yr) at this depth range for area extrapolation. The diffusive Nd flux in the whole East China Sea shelf is $3.0 \pm 0.4 \times 10^4$ mol/yr, higher than the riverine input. Furthermore, on the continental shelf, with dynamic hydraulic environments, advection via *e.g.*, bio-irrigation, rather than diffusion, may play the dominant role in benthic flux of trace metals (Shi *et al.*, 2019), implying a higher benthic flux. The benthic Nd flux accounting for advection processes can be estimated using Equations S-7 and S-8 (Shi *et al.*, 2019). The area-extrapolated advective Nd flux ($30.8 \pm 4.0 \times 10^4$ mol/yr; Table S-5) is ~10-fold higher than the diffusion-based estimate and becomes the largest source on the East China Sea shelf (38 % of the total input).

Our observations and calculations emphasise the role of benthic processes in the Nd cycling of marginal seas, and can provide valuable insights on the global sedimentary Nd flux. The best estimate so far (Abbott *et al.*, 2015; Du *et al.*, 2020) suggests a global benthic Nd flux of 115×10^6 mol/yr, assuming the dominance of diffusion process. However, advection may play a key role in the benthic Nd flux from the continental shelf (0–200 m). Hence, we can revise the shelf estimate by replacing it (~32 pmol/cm^2/yr) with our advection-based estimate (~62 pmol/cm^2/yr), considering that the average depth of our studied shelf (72 m) is close to the global average shelf depth (~60 m) and most global observations (73 %; World Ocean Database 2018, Boyer *et al.*, 2018) on shelves show a bottom water DO within our studied range (Table S-1). Despite the implied increase in the shelf-derived flux, the continental shelf only accounts for 14 % of the global area-integrated benthic Nd flux. This contrasts with previous thoughts that the sedimentary source is mainly from shallow water depths (*e.g.*, continental shelves); in fact, much more extensive deep oceans may dominate the benthic Nd source (Haley *et al.*, 2017; Du *et al.*, 2020). We thus suggest that future ocean models should reconsider the spatial pattern of this sedimentary source. Our results highlight the need for precise constraints on the benthic source if REE/Nd isotopes are to be robustly used as process/source tracer in both marginal seas and on global scales.

Acknowledgements

This work was funded by the National Natural Science Foundation of China (Grant Nos. 42006059, 41991324 and

41730531). J.D. was supported by the ETH Zurich Postdoctoral Fellowship 19-2 FEL-32. K.D. thanks the support by the ETH Zurich Postdoctoral Fellowship 20-1 FEL-24. We thank the crew of the Zheyuke-2, Ni Su, Qi Jia and Zhongya Hu for their assistance with field sampling, Yi Sun for providing DO data, Madalina Jaggi for her assistance with TOC analysis, Jörg Rickli, Tim Jesper Suhrhoff and Archer Corey for their help with lab work.

Editor: Eric Oelkers

Additional Information

Supplementary Information accompanies this letter at https://www.geochemicalperspectivesletters.org/article2223.

Cite this letter as: Deng, K., Yang, S., Du, J., Lian, E., Vance, D. (2022) Dominance of benthic flux of REEs on continental shelves: implications for oceanic budgets. *Geochem. Persp. Let.* 22, 26–30. https://doi.org/10.7185/geochemlet.2223

References

Abbott, A.N., Haley, B.A., McManus, J., Reimers, C.E. (2015) The sedimentary flux of dissolved rare earth elements to the ocean. *Geochimica et Cosmochimica Acta* 154, 186–200. https://doi.org/10.1016/j.gca.2015.01.010

Abbott, A.N., Haley, B.A., McManus, J. (2016) The impact of sedimentary coatings on the diagenetic Nd flux. *Earth and Planetary Science Letters* 449, 217–227. https://doi.org/10.1016/j.epsl.2016.06.001

Arsouze, T., Dutay, J.C., Lacan, F., Jeandel, C. (2009) Reconstructing the Nd oceanic cycle using a coupled dynamical – biogeochemical model. *Biogeosciences* 6, 2829–2846. https://doi.org/10.5194/bg-6-2829-2009

Blaser, P., Lippold, J., Gutjahr, M., Frank, N., Link, J.M., Frank, M. (2016) Extracting foraminiferal seawater Nd isotope signatures from bulk deep sea sediment by chemical leaching. *Chemical Geology* 439, 189–204. https://doi.org/10.1016/j.chemgeo.2016.06.024

Boyer, T.P., Garcia, H.E., Locarnini, R.A., Zweng, M.M., Mishonov, A.V., Reagan, J.R., Weathers, K.A., Baranova, O.K., Seidov, D., Smolyar, I.V. (2018) World Ocean Atlas 2018. NOAA National Centers for Environmental Information. Dataset. Accessed November 2021. https://www.ncei.noaa.gov/archive/accession/NCEI-WOA18

Byrne, R.H., Kim, K.-H. (1993) Rare earth precipitation and coprecipitation behavior: The limiting role of PO_4^{3-} on dissolved rare earth concentrations in seawater. *Geochimica et Cosmochimica Acta* 57, 519–526. https://doi.org/10.1016/0016-7037(93)90364-3

Chen, Z., Li, J., Shen, H., Zhanghua, W. (2001) Yangtze River of China: historical analysis of discharge variability and sediment flux. *Geomorphology* 41, 77–91. https://doi.org/10.1016/S0169-555X(01)00106-4

Du, J., Haley, B.A., Mix, A.C. (2016) Neodymium isotopes in authigenic phases, bottom waters and detrital sediments in the Gulf of Alaska and their implications for paleo-circulation reconstruction. *Geochimica et Cosmochimica Acta* 193, 14–35. https://doi.org/10.1016/j.gca.2016.08.005

Du, J., Haley, B.A., Mix, A.C., Walczak, M.H., Praetorius, S.K. (2018) Flushing of the deep Pacific Ocean and the deglacial rise of atmospheric CO_2 concentrations. *Nature Geoscience* 11, 749–755. https://doi.org/10.1038/s41561-018-0205-6

Du, J., Haley, B.A., Mix, A.C. (2020) Evolution of the Global Overturning Circulation since the Last Glacial Maximum based on marine authigenic neodymium isotopes. *Quaternary Science Reviews* 241, 106396. https://doi.org/10.1016/j.quascirev.2020.106396

Elderfield, H., Greaves, M.J. (1982) The rare earth elements in seawater. *Nature* 296, 214–219. https://doi.org/10.1038/296214a0

Haley, B.A., Klinkhammer, G.P., McManus, J. (2004) Rare earth elements in pore waters of marine sediments. *Geochimica et Cosmochimica Acta* 68, 1265–1279. https://doi.org/10.1016/j.gca.2003.09.012

Haley, B.A., Du, J., Abbott, A.N., McManus, J. (2017) The Impact of Benthic Processes on Rare Earth Element and Neodymium Isotope Distributions in the Oceans. *Frontiers in Marine Science* 4, 426. https://doi.org/10.3389/fmars.2017.00426

Jeandel, C., Oelkers, E.H. (2015) The influence of terrigenous particulate material dissolution on ocean chemistry and global element cycles. *Chemical Geology* 395, 50–66. https://doi.org/10.1016/j.chemgeo.2014.12.001

Johannesson, K.H., Chevis, D.A., Burdige, D.J., Cable, J.E., Martin, J.B., Roy, M. (2011) Submarine groundwater discharge is an important net source of light and middle REEs to coastal waters of the Indian River Lagoon, Florida, USA. *Geochimica et Cosmochimica Acta* 75, 825–843. https://doi.org/10.1016/j.gca.2010.11.005

Liu, J.P., Li, A.C., Xu, K.H., Velozzi, D.M., Yang, Z.S., Milliman, J.D., DeMaster, D.J. (2006) Sedimentary features of the Yangtze River-derived along-shelf clinoform deposit in the East China Sea. *Continental Shelf Research* 26, 2141–2156. https://doi.org/10.1016/j.csr.2006.07.013

Liu, J., Krom, M.D., Ran, X., Zang, J., Liu, J., Yao, Q., Yu, Z. (2020) Sedimentary phosphorus cycling and budget in the seasonally hypoxic coastal area of Changjiang Estuary. *Science of the Total Environment* 713, 136389. https://doi.org/10.1016/j.scitotenv.2019.136389

Liu, Z., Gan, J., Hu, J., Wu, H., Cai, Z., Deng, Y. (2021) Progress of Studies on Circulation Dynamics in the East China Sea: The Kuroshio Exchanges With the Shelf Currents. *Frontiers in Marine Science* 8, 620910. https://doi.org/10.3389/fmars.2021.620910

Patton, G.M., Francois, R., Weis, D., Hathorne, E., Gutjahr, M., Frank, M., Gordon, K. (2021) An experimental investigation of the acquisition of Nd by authigenic phases of marine sediments. *Geochimica et Cosmochimica Acta* 301, 1–29. https://doi.org/10.1016/j.gca.2021.02.010

Rempfer, J., Stocker, T.F., Joos, F., Dutay, J.-C., Siddall, M. (2011) Modelling Nd-isotopes with a coarse resolution ocean circulation model: Sensitivities to model parameters and source/sink distributions. *Geochimica et Cosmochimica Acta* 75, 5927–5950. https://doi.org/10.1016/j.gca.2011.07.044

Rousseau, T.C.C., Sonke, J.E., Chmeleff, J., van Beek, P., Souhaut, M., Boaventura, G., Seyler, P., Jeandel, C. (2015) Rapid neodymium release to marine waters from lithogenic sediments in the Amazon estuary. *Nature Communications* 6, 7592. https://doi.org/10.1038/ncomms8592

Schijf, J., Christenson, E.A., Byrne, R.H. (2015) YREE scavenging in seawater: A new look at an old model. *Marine Chemistry* 177, 460–471. https://doi.org/10.1016/j.marchem.2015.06.010

Shi, X., Wei, L., Hong, Q., Liu, L., Wang, Y., Shi, X., Ye, Y., Cai, P. (2019) Large benthic fluxes of dissolved iron in China coastal seas revealed by $^{224}Ra/^{228}Th$ disequilibria. *Geochimica et Cosmochimica Acta* 260, 49–61. https://doi.org/10.1016/j.gca.2019.06.026

Siddall, M., Khatiwala, S., van de Flierdt, T., Jones, K., Goldstein, S.L., Hemming, S., Anderson, R.F. (2008) Towards explaining the Nd paradox using reversible scavenging in an ocean general circulation model. *Earth and Planetary Science Letters* 274, 448–461. https://doi.org/10.1016/j.epsl.2008.07.044

Wang, Z.-L., Liu, C.-Q. (2008) Geochemistry of rare earth elements in the dissolved, acid-soluble and residual phases in surface waters of the Changjiang Estuary. *Journal of Oceanography* 64, 407–416. https://doi.org/10.1007/s10872-008-0034-0

Dominance of benthic flux of REEs on continental shelves: implications for oceanic budgets

K. Deng, S. Yang, J. Du, E. Lian, D. Vance

Supplementary Information

The Supplementary Information includes:

- Materials and Methods
- Sediment Geochemistry
- REE Scavenging Along the Salinity Transect
- Calculation of Benthic Nd Flux
- Tables S-1 to S-5
- Figures S-1 to S-5
- Supplementary Information References

Materials and Methods

Study Area

The Changjiang is the largest river basin in China (area: 1.8×10^6 km^2) and the third longest river worldwide. It delivers most of the annual sediment load (~85 %) and water (>70 %) during the wet season (May–October) (Chen *et al*., 2001). The Changjiang River is the dominant sediment source in most of the East China Sea shelf area (Huang *et al*., 2020). The East China Sea is fed by several water masses (Guan, 1994; Chen, 2009; Che and Zhang, 2018) including the Changjiang diluted water, the coastal current, the Taiwan Warm Current and the intrusion of the Kuroshio branch current (Fig. S-1). The East China Sea shelf water is dominated by oxic conditions, with occasional occurrence of seasonal hypoxia. In particular, water column stratification caused by input of low-salinity Changjiang diluted water and intrusion of nearshore Kuroshio branch current in summer can impede vertical exchange of dissolved oxygen, leading to hypoxia in the bottom layer of seawater (Zhu *et al*., 2016).

Sampling

During the KECES (Key Elements Cycling in the Changjiang-Estuary-Shelf Transect) cruise in August 2020, we retrieved sediment cores at four locations (water depth: 6–46 m) using a multi-corer. Cores were sampled on board shortly after collection to minimise any oxidation of the porewaters. Overlying water in each core was drained through a hole above the sediment–water interface. Porewater was then extracted *in situ* by inserting pre-cleaned Rhizon samplers (0.15 μm) attached to syringes into the sediment *via* pre-drilled holes in PVC tubes at cm resolution, to allow simultaneous extraction and to minimise cross-contamination between intervals. The extracted porewater was then transferred to pre-cleaned 30 mL LDPE bottles. Core sediment was sliced at cm resolution after porewater extraction.

In addition, surface and bottom water samples (depths of 1 and 11 m) were collected at the outlet of the Changjiang River for comparison (C1 in Fig. S-1). Porewaters and filtered estuarine water samples (using 0.45 μm filters) were acidified to pH < 2 using concentrated HCl in the clean laboratory after the cruise, with analysis >1 month after collection to ensure equilibrium. Geographic and environmental information on sampling stations is provided in Table S-1.

REE Separation and Determination

All chemical and analytical experiments were performed at ETH Zürich. REE were pre-concentrated from 5–10 mL porewater or seawater samples using a column with ~100 μL ethylenediaminetriacetic acid chelating resin (Nobias PA1; Sohrin *et al.,* 2008). The resin was pre-cleaned with 1 M HCl and 18.2 MΩ water, and then conditioned with 30 mM ammonium acetate at a pH of 5.5–6.0. Before loading the sample onto the column, concentrated ammonium acetate buffer was added to each sample to reach a final acetic acid concentration of 0.1 M, and the solution pH was adjusted to 5.5–6.0 using concentrated ammonia solution and HCl. The matrix cations, such as Na, Mg, K and Ca, were eluted from the column with 16–20 mL of 30 mM ammonium acetate buffer, and the trace metals including REE were then collected using 4 mL 1 M HCl.

For ICP-MS measurements, the samples were evaporated to dryness and re-dissolved in ~0.6 mL 2 % HNO_3 doped with 100 ppt Rh-Re as internal standard. Prior to the measurements, the Thermo Fisher Element XR was tuned in low resolution mode to optimise the signal size. Oxide formation was monitored (<~4 %) during REE measurement and its contribution to intensity data was corrected. The intensity data were also corrected for machine blank and machine drift. REE concentrations were calculated based on external calibration standards with REE patterns of seawater and PAAS and a concentration gradient. Final REE concentrations were also corrected for procedure blanks, which were put through column chemistry and only accounted for <1 % of the average [REE] of all samples.

The seawater reference material NASS-5 and an in-house Caribbean seawater standard Jstd-1 (Suhrhoff *et al.*, 2019) were processed in each sample batch to assess replicability and accuracy. The relative standard deviation (RSD) of each REE is generally <4 % (n = 5 for each standard). Although no certified REE concentrations are available for either standard, measured REE data of NASS-5 can be compared to literature values compiled by Zheng *et al.* (2015). The deviation of our NASS-5 measurements from compiled literature values is <~6 % for each REE except Tb (10 %). As such, we propagate a relative uncertainty of 10 % to all porewater REE measurements as a conservative estimate. The measured REE patterns of both standards are provided in Figure S-2.

In addition, two REE-related parameters including Ce anomaly (Ce/Ce^*) and HREE/LREE (Behrens *et al.*, 2018) are calculated after normalisation to PAAS. The equations are shown below.

$$(Ce/Ce^*)_{PAAS} = [Ce]_{PAAS}/(0.5[La]_{PAAS} + 0.5[Pr]_{PAAS}) \quad \text{Eq. S-1}$$

$$(HREE/LREE)_{PAAS} = ([Tm]_{PAAS} + [Yb]_{PAAS} + [Lu]_{PAAS})/([La]_{PAAS} + [Pr]_{PAAS} + [Nd]_{PAAS}) \quad \text{Eq. S-2}$$

Elemental and TOC Analysis

Water and sediment samples were analysed for concentrations of some other elements. An aliquot of each water sample was diluted ~40 times for the determination of elemental concentrations. Sediment samples were rinsed with Milli-Q water twice to remove the salt and then dried in an oven at 60 °C. About 100 mg of powdered sediment was weighed and digested on a hotplate at up to 150 °C using concentrated HF-HNO_3 and aqua regia repeatedly. Finally, the samples were brought up in 2 % HNO_3 and doped with 1 ppb indium (In) as an internal standard for elemental analysis. Elemental concentrations were measured using the Thermo Fisher Element XR. Accuracy and precision were assessed using a secondary multi-element standard from the National Research Council of Canada river standard SLRS5. The measured concentrations agree with certified values within ~10 %. Total organic carbon (TOC) content of the sediment was measured using an Elemental Analyser, after addition of dilute HCl to remove inorganic carbon; repeat analyses of certified standards and samples indicate an RSD of <2 %.

Sediment Geochemistry

The element concentration data (including REE) in water and sediment samples are provided in Tables S-2 and S-3, respectively. In particular, geochemical parameters measured in solid phases are shown in Figure S-5. For sediment parameters such as Nd/Al, Fe/Al and TOC, the down-core and inter-core variability is generally small except at C6-1 (Fig. S-5). The large variation of sediment geochemistry at C6-1 may be related to the dynamic depositional environment at shallow water depth (6 m) and thus short-term changes in physical features of sediments. Furthermore, Mn/Al of surface sediment clearly decreases with water depth and the Changjiang-normalised values, *i.e.* $(Mn/Al)_{CJ}$, are mostly lower than 1. This suggests depletion of Mn compared to its riverine source, which can partially be explained by the diffusive loss of Mn from sediments via porewater (Fig. 2).

REE Scavenging Along the Salinity Transect

We here investigate dissolved REE behaviour in the Changjiang estuary based on salinity transect data collected in 2020 (this study) and in 1998 (Wang and Liu, 2008). The estuarine REE pattern becomes more HREE-enriched from a salinity of <1 psu to higher salinity (solid *vs*. dashed lines; Fig. S-3a), together with the build-up of negative Ce anomaly. This evolution is consistent for each transect and is probably driven by scavenging via colloid coagulation, that preferentially removes LREE, especially Ce (Goldstein and Jacobsen, 1988).

Nd, representative of the LREE, dramatically decreases in concentration at salinity of <1–2 psu (Fig. S-3). To quantify Nd removal in the estuary, we calculate change in sample [Nd] relative to that caused by conservative mixing (Boyle *et al.*, 1974) between end-members of river water ($[Nd]_{riv}$) and seawater ($[Nd]_{sw}$). End-members are shown in Figure S-3 and include the Changjiang downstream water (Wang and Liu, 2008) and East China Sea shelf bottom water (salinity of 33.9; Luong *et al.*, 2018). Specifically, the water mass contribution from seawater (Pct_{sw}, %) to a given estuarine sample can be calculated based on salinity. Next, Nd sourced from the river end-member in a sample ($[Nd]_{riv\text{-}origin}$) is calculated as follows:

$$[Nd]_{riv\text{-}origin} = [Nd]_{sample} - Pct_{sw} \times [Nd]_{sw} \quad \text{Eq. S-3}$$

The Nd removal (RM, %) is then derived from the difference between river-sourced Nd calculated by Equation S-3 and that calculated by conservative mixing:

$$RM = \left(1 - \frac{[Nd]_{riv\text{-}origin}}{(1 - Pct_{sw}) \times [Nd]_{riv}}\right) \times 100 \quad \text{Eq. S-4}$$

According to Equations S-3 and S-4, the low-salinity data (1–10 psu) imply 57 ± 6 % (n = 11) removal of dissolved Nd. Although such a scavenging efficiency is lower than that in the larger Amazon River (93–97 %), it falls within the range for estuarine transects globally (71 ± 16 %; n = 15) (Rousseau *et al.*, 2015). Furthermore, $[Nd]_{diss}$ increases offshore at mid-high salinity (*e.g.,* 10–20 psu; Fig. S-3b) and corresponds to a decrease in scavenging efficiency (14 % in 1998; 22 % in 2020), hinting at addition from a potential marine sedimentary source.

Calculation of Benthic Nd Flux

Early diagenetic reactions and solute diffusion in the sediment column can produce a measurable gradient in dissolved [Nd]. Such a gradient can be used to quantify the diffusive flux of Nd ($J_{Nd\text{-}diff}$) following Fick's first law of diffusion (Boudreau, 1997):

$$J_{Nd\text{-}diff} = \varphi \times D_{Nd}^{sed} \times \frac{\partial C_{Nd}}{\partial z} \quad \text{Eq. S-5}$$

where $\frac{\partial C_{Nd}}{\partial z}$ is the maximum concentration gradient of Nd (mol/L/cm) to the surface in a porewater profile, φ is the porosity (assuming as a constant of 0.9), and D_{Nd}^{sed} is the effective diffusion coefficient of Nd in sediments (cm^2/s). D_{Nd}^{sed} is related to the diffusion coefficient of Nd in seawater (D_{Nd}^{sw} in cm^2/s) and tortuosity and can be calculated as follows (Boudreau, 1997):

$$D_{Nd}^{sed} = \frac{D_{Nd}^{sw}}{1 - \ln(\varphi^2)} \quad \text{Eq. S-6}$$

While D_{Nd}^{sw} is not available, molecular diffusion coefficients for La^{3+} and Yb^{3+} in seawater have been reported previously (Li and Gregory, 1974). Hence, a linear extrapolation from D_{La}^{sw} to D_{Yb}^{sw} based on their atomic order (La as 1 and Yb as 13) is applied to calculate D_{Nd}^{sw} (Abbott *et al.*, 2015) and the effect of water temperature on D^{sw} is corrected for (Li and Gregory, 1974). Note that we use 25 °C for our East China Sea dataset and the results are provided in Table S-4.

In an advection-dominated setting, additional processes over and above diffusion, such as bio-irrigation, can dominate solute exchange across the sediment–water interface. As such, the advective Nd flux ($J_{Nd\text{-}add}$) can be calculated using the following equation modified from Shi *et al.* (2019):

$$J_{Nd\text{-}add} = v \times \Delta[Nd] \quad \text{Eq. S-7}$$

where Δ[Nd] represents the concentration difference between upper-most porewater (1 cm) and bottom seawater and v stands for the interfacial water exchange rate (in $m^3/m^2/d$). Shi *et al.* (2019) proposed an exponential relationship between water depth (Z in m) and v determined by $^{224}Ra/^{228}Th$ disequilibria around our study region (Eq. S-8). Note that this equation yields a relatively stable value of v (around 0.04 $m^3/m^2/d$) when $Z > 40$ m.

$$v = 0.04 + 0.8e^{-0.13Z} \quad \text{Eq. S-8}$$

The advective Nd flux on the East China Sea shelf is calculated by multiplying the mean gradient in $[Nd]_{diss}$ at the sediment–water interface from stations at ≥12 m with the advective water flux derived from its relation with water depth (Eq. S-8) and the average shelf depth (72 m).

Supplementary Tables

Table S-1 Basic characteristics of sampling stations.

Station	Longitude	Latitude	Water Depth	Salinity[b]	Bottom dissolved O_2
	°E	°N	m	psu	μmol/L
C1[a]	121.102	31.766	13	0.2	396
C6-1	122.042	31.068	6	14	304
C10	122.450	30.968	12	20	306
C13	122.886	30.803	33	29	115
B14	122.868	30.101	46	27	203

[a] C1 is a water column station and samples were collected at depths of 1 and 11 m.
[b] The salinity is converted from measured dissolved [K] of bottom water.

Table S-2 Porewater REE and selected element concentrations[a].

Station	Core depth	La	Ce	Pr	Nd	Sm	Eu	Gd	Tb	Dy	Ho	Er	Tm	Yb	Lu	Fe	Mn	P
	cm	ppt	ppt	ppt	ppt	ppt	ppt	ppt	ppt	ppt	ppt	ppt	ppt	ppt	ppt	ppm	ppm	ppm
C6-1	0	10.68	7.43	1.41	6.48	1.50	0.39	2.91	0.35	2.60	0.67	2.27	0.33	2.22	0.39	0.00	0.00	0.00
C6-1	1	7.37	7.69	1.29	5.94	1.36	0.35	2.81	0.33	2.33	0.62	2.04	0.30	2.04	0.34	0.00	0.27	0.02
C6-1	2	8.60	11.84	1.58	7.28	1.75	0.46	3.49	0.40	2.85	0.74	2.40	0.35	2.32	0.39	0.00	2.20	0.03
C6-1	4	8.51	12.83	1.71	7.80	2.00	0.52	4.14	0.46	3.25	0.83	2.72	0.40	2.77	0.44	0.00	2.62	0.04
C6-1	7	13.29	20.98	2.42	10.96	2.39	0.69	4.68	0.48	3.29	0.81	2.60	0.37	2.51	0.42	0.00	4.27	0.02
C6-1	9	18.10	29.78	3.40	15.10	3.38	0.93	5.68	0.68	4.62	1.13	3.42	0.49	3.28	0.54	0.00	5.46	0.02
C6-1	11	13.42	19.56	2.56	12.11	2.94	\	5.03	0.63	4.48	1.08	3.41	0.48	3.28	0.53	0.00	5.09	0.02
C6-1	17	25.06	41.49	4.57	20.80	4.79	1.24	7.91	1.06	7.38	1.83	5.59	0.79	5.25	0.84	0.00	6.06	0.07
C6-1	21	17.50	27.21	3.26	15.91	3.98	1.05	6.46	0.93	6.80	1.73	5.59	0.81	5.55	0.91	5.31	6.20	0.29
C10	0	6.17	3.67	1.15	5.13	1.20	0.31	1.88	0.29	2.16	0.55	1.83	0.26	1.74	0.30	0.00	0.00	0.00
C10	1	13.24	21.60	2.45	11.17	2.69	0.71	4.61	0.67	4.93	1.25	3.99	0.57	3.82	0.60	0.00	4.56	0.02
C10	3	16.67	24.42	2.83	12.68	2.95	0.76	4.95	0.69	4.99	1.25	3.89	0.55	3.70	0.58	0.00	4.14	0.04
C10	4	16.06	26.11	2.83	12.82	3.02	0.80	4.64	0.71	4.99	1.21	3.84	0.54	3.48	0.58	0.00	6.08	0.03
C10	6	21.05	33.93	3.57	16.05	3.67	0.95	6.03	0.83	5.87	1.45	4.43	0.63	4.18	0.66	0.01	8.94	0.06
C10	7	22.81	34.10	3.20	14.28	3.07	0.78	5.07	0.68	4.85	1.23	3.87	0.55	3.76	0.61	1.42	7.20	0.10
C10	9	10.69	15.06	1.26	5.85	1.41	0.34	2.43	0.34	2.52	0.68	2.25	0.33	2.42	0.43	11.79	4.01	0.46
C10	12	8.86	10.68	0.96	4.75	1.10	0.31	2.12	0.35	2.47	0.67	2.32	0.35	2.54	0.47	16.75	5.08	0.41
C10	16	4.57	5.23	0.56	2.91	0.97	0.22	1.66	0.26	1.89	0.58	2.07	0.32	2.38	0.44	18.86	4.93	0.75
C10	25	4.91	6.69	0.70	3.31	1.08	0.23	1.61	0.26	2.13	0.61	2.10	0.32	2.38	0.42	5.54	2.82	0.15
C13	0	8.37	2.59	1.31	5.82	1.32	0.34	2.10	0.33	2.48	0.63	2.07	0.29	1.95	0.32	0.01	0.00	0.00
C13	1	16.21	23.74	2.51	11.12	2.54	0.62	3.97	0.57	4.01	0.96	3.03	0.42	2.85	0.46	0.01	6.52	0.05
C13	2	16.56	21.15	1.73	7.85	1.55	0.37	2.55	0.36	2.52	0.64	2.05	0.29	2.07	0.37	5.29	8.91	0.24
C13	3	16.76	24.69	2.09	9.45	1.99	0.49	3.15	0.45	3.06	0.76	2.40	0.35	2.45	0.42	5.94	9.20	0.39
C13	4	21.63	32.54	3.11	13.49	2.76	0.69	3.79	0.56	3.88	0.93	2.99	0.42	2.78	0.49	5.87	5.06	0.41
C13	7	13.38	18.19	1.60	7.35	1.49	0.38	2.48	0.37	2.58	0.66	2.14	0.31	2.13	0.39	2.45	1.55	0.29

Table S-2 continued.

Station	Core depth	La	Ce	Pr	Nd	Sm	Eu	Gd	Tb	Dy	Ho	Er	Tm	Yb	Lu	Fe	Mn	P
	cm	ppt	ppt	ppt	ppt	ppt	ppt	ppt	ppt	ppt	ppt	ppt	ppt	ppt	ppt	ppm	ppm	ppm
C13	9	8.61	9.02	0.77	3.55	0.81	0.18	1.26	0.20	1.44	0.40	1.40	0.21	1.50	0.29	3.35	1.43	0.47
C13	11	8.68	10.52	0.95	4.53	0.91	0.23	1.54	0.22	1.63	0.44	1.50	0.22	1.50	0.28	1.60	1.06	0.30
C13	17	4.90	5.69	0.52	2.49	0.60	0.14	0.94	0.14	1.10	0.31	1.07	0.16	1.21	0.23	1.27	1.20	0.42
C13	21	7.18	9.15	0.91	4.23	1.05	0.24	1.47	0.24	1.80	0.49	1.69	0.25	1.82	0.33	0.58	1.01	0.27
B14	0	9.52	4.32	1.50	6.72	1.47	0.38	2.18	0.34	2.53	0.63	2.00	0.28	1.78	0.29	0.00	0.00	0.02
B14	1	19.61	22.54	3.02	13.61	2.91	0.75	4.32	0.65	4.51	1.07	3.32	0.46	2.92	0.49	0.00	0.51	0.07
B14	2	23.31	28.46	2.52	11.28	2.20	0.54	3.31	0.47	3.25	0.81	2.56	0.36	2.33	0.41	1.71	1.10	0.12
B14	5	10.08	13.97	1.33	6.28	1.36	0.36	2.27	0.35	2.60	0.67	2.24	0.33	2.23	0.40	1.22	1.87	0.53
B14	6	28.69	35.09	3.02	13.48	2.48	0.62	3.79	0.52	3.70	0.92	2.95	0.41	2.65	0.48	3.08	2.58	0.25
B14	7	8.05	11.70	1.10	5.22	1.19	0.31	1.97	0.30	2.23	0.59	1.98	0.29	2.02	0.38	0.60	1.92	0.63
B14	11	9.67	15.45	1.48	6.99	1.62	0.42	2.51	0.39	2.82	0.71	2.30	0.33	2.24	0.40	0.20	1.27	1.18
B14	15	5.73	8.68	0.84	3.97	0.96	0.25	1.50	0.24	1.78	0.47	1.58	0.23	1.59	0.30	0.33	1.11	1.30
B14	19	7.11	10.15	0.94	4.47	1.05	0.27	1.68	0.26	1.97	0.52	1.72	0.26	1.83	0.33	1.46	1.15	0.74
C1-1[b]		7.87	10.61	1.86	8.54	1.96	0.46	3.01	0.34	2.36	0.56	1.75	0.25	1.64	0.28	0.00	0.00	0.04
C1-11[b]		6.90	9.23	1.67	7.59	1.83	0.44	2.95	0.33	2.26	0.53	1.70	0.24	1.58	0.27	0.00	0.00	0.04

[a] A relative uncertainty of 10 % is applied for all element measurements.

[b] C1-1 and C1-11 are water samples in the Changjiang outlet collected at water depths of 1 and 11 m, respectively.

Table S-3 Core sediment REE and selected element concentrations.

Station	Core depth	La	Ce	Pr	Nd	Sm	Eu	Gd	Tb	Dy	Ho	Er	Tm	Yb	Lu	Fe	Mn	Al	TOC
	cm	ppb	ppb	ppb	ppb	ppb	ppb	ppb	ppb	ppb	ppb	ppb	ppb	ppb	ppb	ppm	ppm	ppm	%
C6-1	0.5	40122	79956	9145	34129	6634	1375	5811	881	5235	1020	2911	411	2745	397	41720	1072	76175	0.77
C6-1	1.5	39862	79278	9108	33960	6594	1359	5738	860	5081	976	2810	394	2647	386	37145	929	64697	0.58
C6-1	2.5	43934	87865	10217	37977	7296	1417	6065	922	5462	1063	3022	417	2716	377	25615	574	40621	0.10
C6-1	3.5	48758	94879	10827	39821	7286	1387	5959	841	4828	907	2564	353	2411	351	30559	687	48203	0.40
C6-1	6.5	40194	80185	9264	34761	6540	1261	5307	762	4376	824	2307	320	2099	302	25497	560	46047	0.20
C6-1	8.5	72314	141974	16166	58638	10545	1691	8395	1106	6088	1122	3124	429	2848	413	30630	711	40079	0.09
C6-1	10.5	23944	47953	5636	21219	4123	941	3516	526	3094	583	1653	229	1569	218	19993	437	42589	0.09
C6-1	16.5	36938	72011	8361	31525	6165	1264	5340	821	4851	929	2648	374	2489	357	23697	512	44262	0.15
C6-1	21.0	38723	75804	8896	33072	6237	1192	5177	778	4614	901	2603	366	2473	362	26133	619	52142	0.36
C10	0.5	40834	81282	9294	34701	6737	1381	5850	905	5450	1064	3055	431	2873	420	39681	944	77588	0.67
C10	1.5	38612	77017	8852	33076	6428	1324	5569	871	5230	1026	2974	413	2797	405	38902	909	74242	0.69
C10	2.5	38381	76400	8791	33011	6392	1322	5543	862	5139	1002	2889	404	2672	393	36932	878	71809	0.64
C10	3.5	36294	71789	8370	31219	6075	1232	5202	799	4807	937	2718	382	2535	367	30443	716	59617	0.40
C10	5.5	36042	71431	8328	31191	6093	1241	5272	814	4906	955	2776	389	2590	370	30441	669	58196	0.40
C10	6.5	35105	70058	8114	30452	5886	1201	4999	777	4689	920	2638	368	2451	358	30253	640	62638	0.36
C10	8.5	37580	74870	8650	32397	6222	1227	5143	782	4688	909	2607	365	2445	355	29960	642	60708	0.36
C10	11.5	37323	74561	8541	31835	6153	1257	5319	822	4960	978	2801	393	2614	380	32384	679	66518	0.38
C10	15.5	39302	78345	9030	33742	6477	1290	5539	843	5035	980	2800	392	2626	379	32893	640	65372	0.41
C10	24.5	40397	80448	9244	34458	6690	1359	5747	876	5215	1014	2920	407	2716	393	38586	839	76659	0.50
C13	0.5	37337	74353	8565	31955	6171	1255	5299	814	4898	955	2746	384	2557	370	33407	727	68343	0.53
C13	1.5	37494	74763	8574	31906	6138	1231	5196	791	4733	922	2671	372	2489	362	33432	663	68385	0.53
C13	2.5	37142	73928	8472	31806	6170	1260	5327	822	5030	974	2821	392	2620	383	36283	715	73182	0.57
C13	3.5	38962	77535	8962	33326	6479	1305	5480	831	4965	970	2786	388	2605	382	33868	645	69154	0.53
C13	4.5	36682	72712	8447	31602	6135	1244	5142	802	4793	932	2674	375	2505	364	33557	669	69174	0.54

Table S-3 continued.

Station	Core depth	La	Ce	Pr	Nd	Sm	Eu	Gd	Tb	Dy	Ho	Er	Tm	Yb	Lu	Fe	Mn	Al	TOC
	cm	ppb	ppb	ppb	ppb	ppb	ppb	ppb	ppb	ppb	ppb	ppb	ppb	ppb	ppb	ppm	ppm	ppm	%
C13	6.5	37261	74285	8542	31934	6145	1252	5213	806	4840	943	2734	382	2537	369	36215	649	73982	0.56
C13	8.5	37092	74066	8533	31953	6214	1278	5330	826	4988	971	2774	391	2615	381	35568	666	72429	0.51
C13	10.5	37006	74018	8534	31831	6145	1263	5246	808	4894	952	2741	383	2543	369	35851	663	72748	0.51
C13	16.5	37609	75941	8744	32921	6365	1264	5479	845	5084	989	2827	393	2611	379	31717	601	65317	0.42
C13	20.5	36329	72147	8344	31574	6187	1242	5155	796	4755	927	2668	376	2509	364	33957	625	68568	0.50
B14	0.5	39275	78267	8924	33286	6292	1254	5287	797	4731	921	2645	370	2466	361	37864	647	76362	0.60
B14	1.5	41469	81304	9052	33041	6148	1230	5145	775	4575	884	2536	352	2358	340	35766	591	70607	0.51
B14	2.5	34676	69334	7935	29688	5686	1191	4803	738	4388	852	2445	338	2255	327	34227	595	68641	0.50
B14	3.5	36814	73442	8461	31781	6160	1268	5226	800	4784	931	2663	372	2482	358	36023	627	73423	0.54
B14	4.5	37047	74763	8572	31998	6211	1267	5273	803	4795	925	2648	372	2470	358	35284	621	71825	0.49
B14	5.5	34232	68627	7852	29379	5715	1196	4822	741	4426	860	2452	342	2282	333	34491	590	70109	0.49
B14	6.5	40873	81153	9277	34541	6595	1342	5614	879	5254	1024	2919	411	2735	400	37635	645	75155	0.58
B14	8.5	39112	78815	9036	33690	6446	1337	5383	823	4907	941	2687	375	2486	365	37932	654	76136	0.55
B14	10.5	38974	77683	8864	32973	6268	1290	5261	795	4737	918	2624	368	2451	360	36112	645	70512	0.53
B14	14.5	37200	74714	8561	31956	6145	1283	5262	812	4944	963	2787	390	2607	378	38461	657	75170	0.52
B14	18.5	38065	76918	8814	32955	6308	1298	5344	812	4826	940	2683	375	2491	360	36542	604	72004	0.44

Note: A relative uncertainty of 10 % is applied for all element measurements and 2 % for TOC analysis.

Table S-4 Diffusive sedimentary Nd fluxes compiled from literature. Footnotes are on the following page.

Station	Basin	Lat.[a]	Long.[a]	Water depth	T^b	Bottom O_2[c]	Nd gradient[d]	Uncertainty	D_s[e]	Diffusive Nd flux[e]	Uncertainty[f]	Reference
		°N	°E	m	°C	µmol/L	pmol/L/cm	pmol/L/cm	cm²/s	pmol/cm²/yr	pmol/cm²/yr	
C6-1	East China Sea	31.1	122.0	6	25.0	304	6.5	1.3	5.03E-06	0.9	0.2	This study
C10	East China Sea	31.0	122.5	12	25.0	306	41.8	8.5	5.03E-06	6.0	1.2	This study
C13	East China Sea	30.8	122.9	33	25.0	115	36.8	8.7	5.03E-06	5.2	1.2	This study
B14	East China Sea	30.1	122.9	46	25.0	203	47.8	10.5	5.03E-06	6.8	1.5	This study
SoG	Strait of Georgia	49.2	-123.5	251	9.0	156	74.9	12.2	3.22E-06	6.8	1.1	Patton *et al.* (2021)
PH150[g]	Tasman Sea	-34.1	151.2	150						12.5	*2.5*	Abbott (2019)
JB1500[g]	Tasman Sea	-34.5	151.2	1550						25.1	*5.0*	Abbott (2019)
HH200	Oregon/California margin	43.9	-124.7	202	7.0	71	*17.9*	11.3	2.99E-06	1.5	1.0	Abbott *et al.* (2015)
HH500	Oregon/California margin	43.9	-124.9	500	5.0	32	183.3	30.3	2.76E-06	14.4	2.4	Abbott *et al.* (2015)
HH1200	Oregon/California margin	43.8	-125.0	1216	4.0	20	220.1	37.0	2.65E-06	16.6	2.8	Abbott *et al.* (2015)
HH3000	Oregon/California margin	43.9	-125.6	3060	2.0	82	237.9	43.5	2.42E-06	16.4	3.0	Abbott *et al.* (2015)
Station 1	Oregon/California margin	43.9	-124.3	105	9.0	78	*19.4*	28.3	3.22E-06	1.8	2.6	Abbott *et al.* (2015)
Station 2	Oregon/California margin	43.9	-124.7	192	7.0	64	*495.5*	126.2	2.99E-06	42.0	10.7	Abbott *et al.* (2015)
Station 3	Oregon/California margin	41.0	-124.3	95	9.0	142	*362.2*	118.2	3.22E-06	33.1	10.8	Abbott *et al.* (2015)
Station 6	Oregon/California margin	41.0	-124.3	125	8.0	125	*252.4*	89.6	3.10E-06	22.2	7.9	Abbott *et al.* (2015)
HRN	Northeast Pacific	44.7	-125.1	600	*4.7*	*23*	109.1	17.5	2.73E-06	8.5	1.4	Himmler *et al.* (2013)
HRS	Northeast Pacific	44.6	-125.1	768	*4.1*	*18*	179.1	25.5	2.66E-06	13.5	1.9	Himmler *et al.* (2013)
Sta. 8	California margin	35.4	-121.4	800	*4.6*	14	880.5	141.2	2.71E-06	67.8	10.9	Haley *et al.* (2004)
Sta. 9	California margin	35.6	-122.1	1600	*2.6*	54	527.1	97.7	2.49E-06	37.3	6.9	Haley *et al.* (2004)
Sta. 10	California margin	36.1	-122.6	3400	*4.0*	128	1082.4	262.1	2.65E-06	81.4	19.7	Haley *et al.* (2004)
MC64	Peru margin	-17.0	-78.1	2930	*1.8*	150	310.0	65.0	2.40E-06	21.1	4.4	Haley *et al.* (2004)
Buzzards Bay	Buzzards Bay	*41.6*	*-70.8*	15	20.0		55.5		4.46E-06	7.0	*1.4*	Sholkovitz *et al.* (1989)
Buzzards Bay	Buzzards Bay	*41.6*	*-70.8*	15	12.0		108.9		3.55E-06	11.0	*2.2*	Elderfield and Sholkovitz (1987)

Table S-4 footnotes.

[a] Latitude/longitude data in italic is roughly estimated from the map.

[b] We adopted a bottom water temperature of 25 °C for the shallow East China Sea shelf based on long-term observation in summer (Chen, 2009). Water temperature data in italic is extracted from World Ocean Database 2018 (https://odv.awi.de/data/ocean/world-ocean-atlas-2018/) based on the location information or assumed as 4 °C.

[c] Bottom water O_2 data in italic is extracted from World Ocean Database 2018 based on the location information.

[d] This is calculated based on the maximum gradient of porewater [Nd] to the surface (bottom water) except numbers in italic for which bottom water [Nd] is not provided and thus the shallowest porewater sample is used.

[e] D_s: diffusion coefficient in sediment. Diffusive Nd flux here is calculated using Equation S-5.

[f] The uncertainty of diffusive flux is propagated from that of the Nd gradient. For numbers in italic, a relative uncertainty of 20 % is arbitrarily propagated to the fluxes as no uncertainty is reported in the literature.

[g] No raw Nd concentration data are provided and thus we simply adopted the reported flux value.

Table S-5 Major sources of dissolved Nd on the East China Sea shelf.

Nd source	$[Nd]_{diss}$ pmol/kg	1 σ pmol/kg	Discharge km^3/yr	Nd flux mol/yr	1 σ mol/yr	Proportion %	Reference[a]
Changjiang River	29.8[b]	4.2	9.00E+02	2.7E+04	3.7E+03	3 %	Wang and Liu (2008); Deng *et al.* (2016)
Atmospheric input	28.8	6.6	5.75E+02	1.7E+04	3.8E+03	2 %	Zhang and Liu (2004); Zhang *et al.* (2005)
Taiwan Strait Current[c]	5.7[d]	1.0	3.78E+04	2.2E+05	3.8E+04	26 %	Luong *et al.* (2018); Liu *et al.* (2021)
Intrusion of the Kuroshio Current	5.7[d]	1.0	4.42E+04	2.5E+05	4.4E+04	31 %	Luong *et al.* (2018); Liu *et al.* (2021)
Shelf benthic flux[e]				3.1E+05	4.0E+04	38 %	This study; Shi *et al.* (2019)

[a] The references for each source are listed as: $[Nd]_{diss}$; Discharge.

[b] $[Nd]_{diss}$ in the Changjiang River here is calculated by accounting for the estuarine removal (57 %).

[c] The Taiwan Strait Current is the north-eastward current through the Taiwan Strait and includes the Taiwan Warm Current and the coastal current.

[d] The major source of both currents is the Kuroshio mainstream (Guan, 1994; Liu *et al.*, 2021), and thus we assume their $[Nd]_{diss}$ as the average value measured from three stations along the Kuroshio mainstream (depth of 0–200 m) (Luong *et al.*, 2018).

[e] The shelf benthic flux is calculated by multiplying the advective Nd flux (61.6 pmol/cm^2/yr; see Eqs. S-7 and S-8 for calculation details) by the shelf area (5×10^5 km^2).

Supplementary Figures

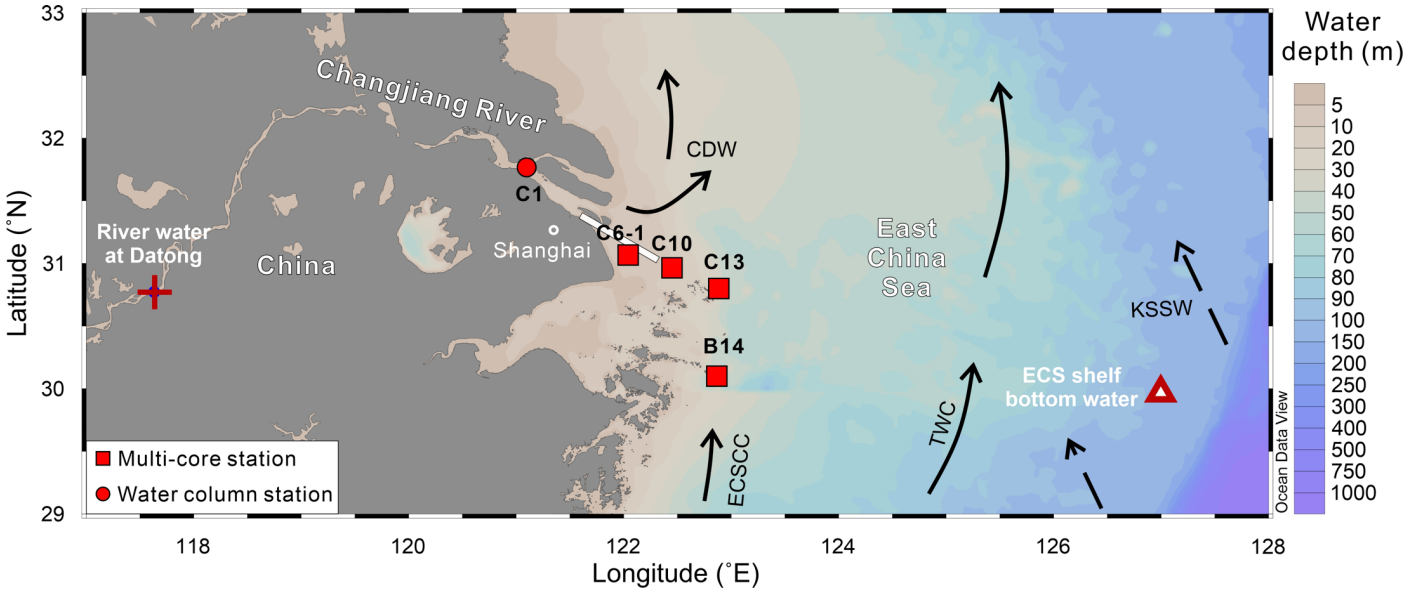

Figure S-1 Sampling stations in the Changjiang Estuary–East China Sea shelf transect. Major water masses in the study area in summer are indicated: CDW, Changjiang Diluted Water; ECSCC, East China Sea Coastal Current; TWC, Taiwan Warm Current; and KSSW, Kuroshio Surface/Subsurface Water (Chen, 2009). ECSCC and TWC can be combined as the Taiwan Strait Current and TWC is mainly sourced from the Kuroshio Current (Guan, 1994). The salinity transect collected in 1998 (Fig. 3) is shown as a white bar in the Changjiang estuary. REE end-members including the Changjiang at Datong station and East China Sea shelf bottom water in Figure 3 are also marked.

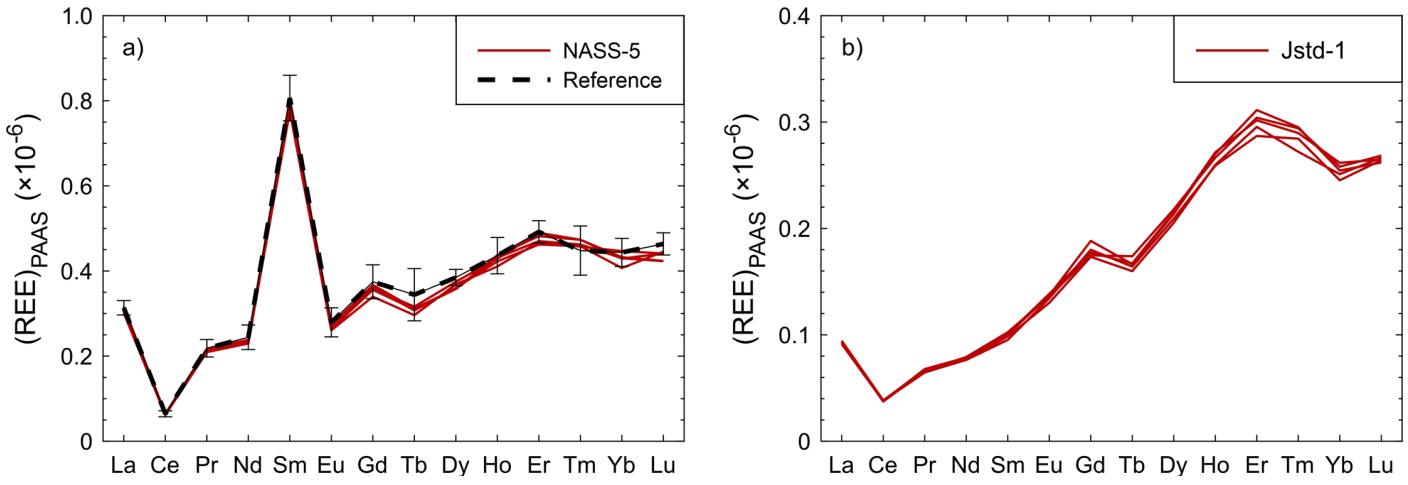

Figure S-2 **(a)** PAAS-normalised REE pattern of the seawater reference material NASS-5 (5 measurements). **(b)** REE pattern of in-house Caribbean seawater standard Jstd-1 (5 measurements). The reference line in **(a)** is the average value and standard deviation of NASS-5 measurements in nine previous studies compiled by Zheng *et al.* (2015). Jstd-1 in **(b)** was adopted as a consistency standard in a previous study (Suhrhoff *et al.*, 2019) but REE data have not been reported before for this sample.

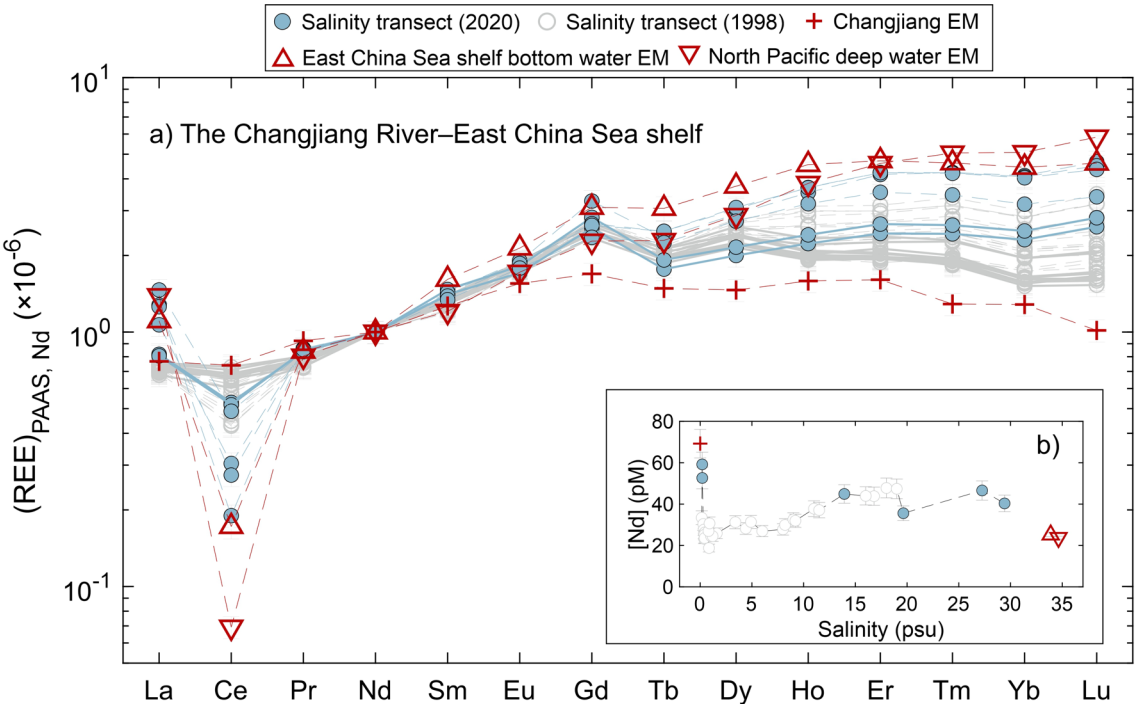

Figure S-3 **(a)** The dissolved REE pattern along the salinity transect of the Changjiang River–East China Sea shelf, normalised first to PAAS and then Nd. **(b)** $[Nd]_{diss}$ along the transect. Transect data in 2020 and in 1998 are from this study and Wang and Liu (2008), respectively. Water mass end-members (EMs) include the Changjiang River (downstream) (Wang and Liu, 2008), East China Sea shelf bottom water (ECSBW, depth: 70–92 m; salinity: 33.9 psu; Luong *et al.*, 2018), and North Pacific deep water (NDPW; depth: 2400–2600 m; Alibo and Nozaki, 1999). Salinity transect data in **(a)** with salinities <1 psu are marked as a solid line.

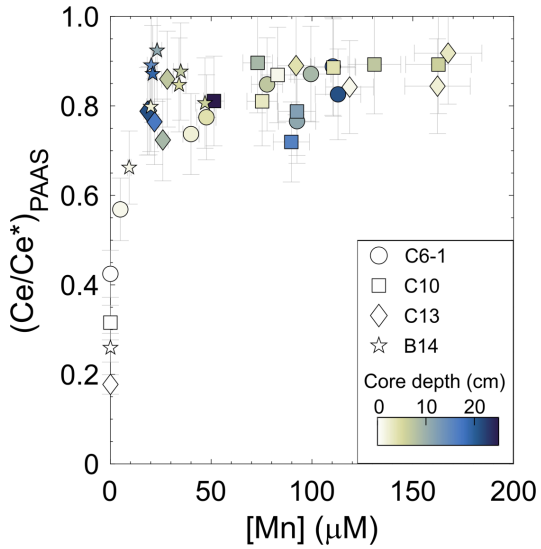

Figure S-4 Porewater [Mn]–Ce/Ce* plot. There is a positive correlation between both parameters for porewater samples at shallow depths (<7 cm) of all stations ($R^2 = 0.44$, $p < 0.01$).

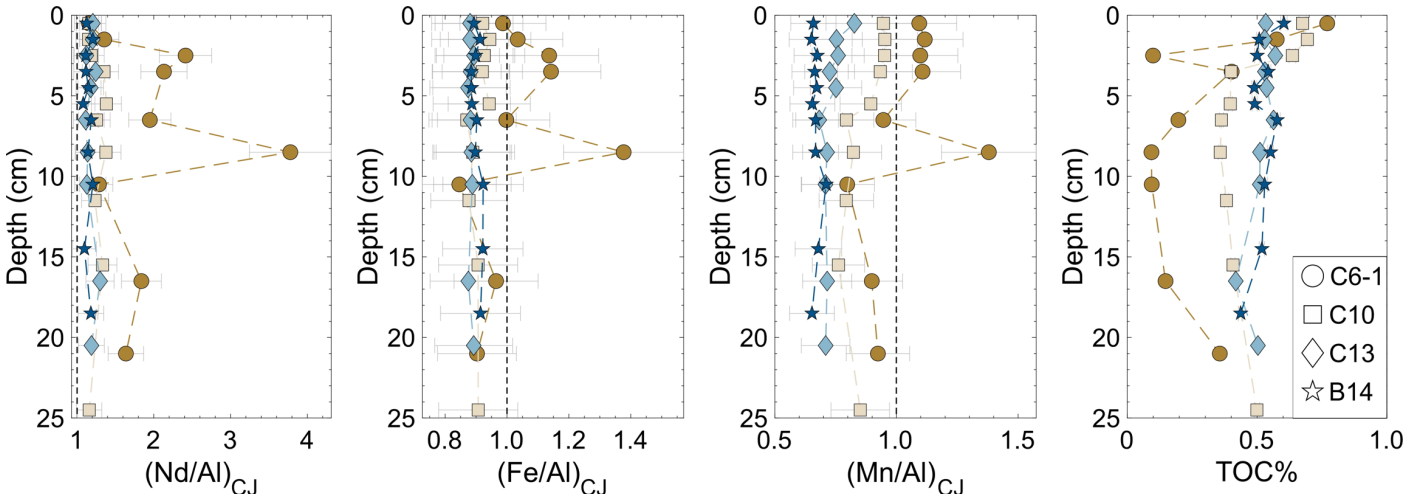

Figure S-5 Geochemical parameters in core sediment (Nd/Al, Fe/Al, Mn/Al, and TOC %). The ratio of element *X* to Al in core sediment is normalised to the ratio in the suspended sediment from the Changjiang (CJ) downstream (Guo *et al.*, 2018).

Supplementary Information References

Abbott, A.N. (2019) A benthic flux from calcareous sediments results in non-conservative neodymium behavior during lateral transport: A study from the Tasman Sea. *Geology* 47, 363–366. https://doi.org/10.1130/G45904.1

Abbott, A.N., Haley, B.A., McManus, J., Reimers, C.E. (2015) The sedimentary flux of dissolved rare earth elements to the ocean. *Geochimica et Cosmochimica Acta* 154, 186–200. https://doi.org/10.1016/j.gca.2015.01.010

Alibo, D.S., Nozaki, Y. (1999) Rare earth elements in seawater: particle association, shale-normalization, and Ce oxidation. *Geochimica et Cosmochimica Acta* 63, 363–372. https://doi.org/10.1016/S0016-7037(98)00279-8

Behrens, M.K., Pahnke, K., Paffrath, R., Schnetger, B., Brumsack, H.-J. (2018) Rare earth element distributions in the West Pacific: Trace element sources and conservative *vs*. non-conservative behavior. *Earth and Planetary Science Letters* 486, 166–177. https://doi.org/10.1016/j.epsl.2018.01.016

Boudreau, B.P. (1997) *Diagenetic models and their implementation*. First Edition, Springer, Berlin.

Boyle, E., Collier, R., Dengler, A.T., Edmond, J.M., Ng, A.C., Stallard, R.F. (1974) On the chemical mass-balance in estuaries. *Geochimica et Cosmochimica Acta* 38, 1719–1728. https://doi.org/10.1016/0016-7037(74)90188-4

Che, H., Zhang, J. (2018) Water Mass Analysis and End-Member Mixing Contribution Using Coupled Radiogenic Nd Isotopes and Nd Concentrations: Interaction Between Marginal Seas and the Northwestern Pacific. *Geophysical Research Letters* 45, 2388–2395. https://doi.org/10.1002/2017GL076978

Chen, C.-T.A. (2009) Chemical and physical fronts in the Bohai, Yellow and East China seas. *Journal of Marine Systems* 78, 394–410. https://doi.org/10.1016/j.jmarsys.2008.11.016

Chen, Z., Li, J., Shen, H., Zhanghua, W. (2001) Yangtze River of China: historical analysis of discharge variability and sediment flux. *Geomorphology* 41, 77–91. https://doi.org/10.1016/S0169-555X(01)00106-4

Deng, K., Yang, S., Lian, E., Li, C., Yang, C., Wei, H. (2016) Three Gorges Dam alters the Changjiang (Yangtze) river water cycle in the dry seasons: Evidence from H-O isotopes. *Science of The Total Environment* 562, 89–97. https://doi.org/10.1016/j.scitotenv.2016.03.213

Elderfield, H., Sholkovitz, E.R. (1987) Rare earth elements in the pore waters of reducing nearshore sediments. *Earth and Planetary Science Letters* 82, 280–288. https://doi.org/10.1016/0012-821X(87)90202-0

Goldstein, S.J., Jacobsen, S.B. (1988) Rare earth elements in river waters. *Earth and Planetary Science Letters* 89, 35–47. https://doi.org/10.1016/0012-821X(88)90031-3

Guan, B.X. (1994) Patterns and Structures of the Currents in Bohai, Huanghai and East China Seas. In: Zhou, D., Liang, Y.-B., Zeng, C.-K. (Eds.) *Oceanology of China Seas*. First Edition, Springer, Dordrecht, 17–26. https://doi.org/10.1007/978-94-011-0862-1_3

Guo, Y., Yang, S., Su, N., Li, C., Yin, P., Wang, Z. (2018) Revisiting the effects of hydrodynamic sorting and sedimentary recycling on chemical weathering indices. *Geochimica et Cosmochimica Acta* 227, 48–63. https://doi.org/10.1016/j.gca.2018.02.015

Haley, B.A., Klinkhammer, G.P., McManus, J. (2004) Rare earth elements in pore waters of marine sediments. *Geochimica et Cosmochimica Acta* 68, 1265–1279. https://doi.org/10.1016/j.gca.2003.09.012

Himmler, T., Haley, B.A., Torres, M.E., Klinkhammer, G.P., Bohrmann, G., Peckmann, J. (2013) Rare earth element geochemistry in cold-seep pore waters of Hydrate Ridge, northeast Pacific Ocean. *Geo-Marine Letters* 33, 369–379. https://doi.org/10.1007/s00367-013-0334-2

Huang, X., Song, J., Yue, W., Wang, Z., Mei, X., Li, Y., Li, F., Lian, E., Yang, S. (2020) Detrital Zircon U-Pb Ages in the East China Seas: Implications for Provenance Analysis and Sediment Budgeting. *Minerals* 10, 398. https://doi.org/10.3390/min10050398

Li, Y.-H., Gregory, S. (1974) Diffusion of ions in sea water and in deep-sea sediments. *Geochimica et Cosmochimica Acta* 38, 703–714. https://doi.org/10.1016/0016-7037(74)90145-8

Liu, Z., Gan, J., Hu, J., Wu, H., Cai, Z., Deng, Y. (2021) Progress of Studies on Circulation Dynamics in the East China Sea: The Kuroshio Exchanges With the Shelf Currents. *Frontiers in Marine Science* 8, 620910. https://doi.org/10.3389/fmars.2021.620910

Luong, L.D., Shinjo, R., Hoang, N., Shakirov, R.B., Syrbu, N. (2018) Spatial variations in dissolved rare earth element concentrations in the East China Sea water column. *Marine Chemistry* 205, 1–15. https://doi.org/10.1016/j.marchem.2018.07.004

Patton, G.M., Francois, R., Weis, D., Hathorne, E., Gutjahr, M., Frank, M., Gordon, K. (2021) An experimental investigation of the acquisition of Nd by authigenic phases of marine sediments. *Geochimica et Cosmochimica Acta* 301, 1–29. https://doi.org/10.1016/j.gca.2021.02.010

Rousseau, T.C.C., Sonke, J.E., Chmeleff, J., van Beek, P., Souhaut, M., Boaventura, G., Seyler, P., Jeandel, C. (2015) Rapid neodymium release to marine waters from lithogenic sediments in the Amazon estuary. *Nature Communications* 6, 7592. https://doi.org/10.1038/ncomms8592

Shi, X., Wei, L., Hong, Q., Liu, L., Wang, Y., Shi, X., Ye, Y., Cai, P. (2019) Large benthic fluxes of dissolved iron in China coastal seas revealed by $^{224}Ra/^{228}Th$ disequilibria. *Geochimica et Cosmochimica Acta* 260, 49–61. https://doi.org/10.1016/j.gca.2019.06.026

Sholkovitz, E.R., Piepgras, D.J., Jacobsen, S.B. (1989) The pore water chemistry of rare earth elements in Buzzards Bay sediments. *Geochimica et Cosmochimica Acta* 53, 2847–2856. https://doi.org/10.1016/0016-7037(89)90162-2

Sohrin, Y., Urushihara, S., Nakatsuka, S., Kono, T., Higo, E., Minami, T., Norisuye, K., Umetani, S. (2008) Multielemental Determination of GEOTRACES Key Trace Metals in Seawater by ICPMS after Preconcentration Using an Ethylenediaminetriacetic Acid Chelating Resin. *Analytical Chemistry* 80, 6267–6273. https://doi.org/10.1021/ac800500f

Suhrhoff, T.J., Rickli, J., Crocket, K., Bura-Nakic, E., Vance, D. (2019) Behavior of beryllium in the weathering environment and its delivery to the ocean. *Geochimica et Cosmochimica Acta* 265, 48–68. https://doi.org/10.1016/j.gca.2019.08.017

Wang, Z.-L., Liu, C.-Q. (2008) Geochemistry of rare earth elements in the dissolved, acid-soluble and residual phases in surface waters of the Changjiang Estuary. *Journal of Oceanography* 64, 407–416. https://doi.org/10.1007/s10872-008-0034-0

Zhang, J., Liu, C.-Q. (2004) Major and rare earth elements in rainwaters from Japan and East China Sea: Natural and anthropogenic sources. *Chemical Geology* 209, 315–326. https://doi.org/10.1016/j.chemgeo.2004.06.014

Zhang, J., Zhang, G.S., Liu, S.M. (2005) Dissolved silicate in coastal marine rainwaters: Comparison between the Yellow Sea and the East China Sea on the impact and potential link with primary production. *Journal of Geophysical Research: Atmospheres* 110, D16304. https://doi.org/10.1029/2004JD005411

Zheng, X.-Y., Yang, J., Henderson, G.M. (2015) A Robust Procedure for High-Precision Determination of Rare Earth Element Concentrations in Seawater. *Geostandards and Geoanalytical Research* 39, 277–292. https://doi.org/10.1111/j.1751-908X.2014.00307.x

Zhu, J., Zhu, Z., Lin, J., Wu, H., Zhang, J. (2016) Distribution of hypoxia and pycnocline off the Changjiang Estuary, China. *Journal of Marine Systems* 154, 28–40. https://doi.org/10.1016/j.jmarsys.2015.05.002